PAPER

Cluster coarsening on drops exhibits strong and sudden size-selectivity

Aidan I. Brown and Andrew D. Rutenberg*

Autophagy, an important process for degradation of cellular components, requires the targeting of autophagy receptor proteins to potential substrates. Receptor proteins have been observed to form clusters on membranes. To understand how receptor clusters might affect autophagy selectivity, we model cluster coarsening on a polydisperse collection of spherical drop-like substrates. Our model receptor corresponds to NBR1, which supports peroxisome autophagy. We recover dynamical scaling of cluster sizes, but find that changing the drop size distribution changes the cluster-size scaling distribution. The magnitude of this effect is similar to how changing the spatial-dimension affects scaling in bulk systems. We also observe a sudden onset of size-selection of the remaining drops with clusters, due to clusters evaporating from smaller drops and growing on larger drops. This coarsening-driven size selection provides a physical mechanism for autophagy selectivity, and may explain reports of size selection during peroxisome degradation.

1 Introduction

Domain coarsening describes multiple clusters growing in average size but decreasing in number, due to the conserved amount of constituents in the system.[1] Biological coarsening has been considered in models of clustering on bacterial membranes[2,3] and for membrane polarization.[4] However, these models have focused only on a single membrane or membrane patch, whereas cells have multiple organelles and hence multiple disconnected surfaces.

Autophagy is an important system for the degradation of large cellular substrates,[5] including protein aggregates, organelles, and pathogenic bacteria. While autophagy was initially described as a non-selective "self-eating" degradation pathway,[6] it is capable of selective substrate degradation. Autophagy substrates are directed to the lysosome for degradation in a multi-stage process that requires receptor protein attachment, and selectivity appears to be mediated by a growing list of autophagy receptor proteins.[7] Although there is a developing understanding of how different receptor proteins select distinct organelles for autophagy,[6,7] *e.g.* peroxisomes *vs.* mitochondria, there has been little investigation of how individual organelles are selected from among a subcellular population. Specifically, what physical cues could lead to the selection of individual organelles?

Peroxisomes are drop-like organelles that range in size[8] from ~ 0.1–0.8 μm, and there can be hundreds in a single mammalian cell.[9] The autophagy of peroxisomes, or pexophagy, can occur after peroxisome proliferation in order to reduce peroxisome

numbers. Intriguingly, this autophagy response varies with peroxisome size.[10,11] This suggests that organelle size might directly affect autophagy selectivity, *i.e.* size may be directly sensed by the autophagy machinery. We explore that possibility in this paper.

Self-interaction of receptor proteins is common. For the NBR1 receptor, which is necessary and sufficient for pexophagy, self-interaction is driven by coiled-coil domains that are essential for normal autophagy.[12] Consistent with self-interaction, domains of receptor proteins have been observed on the surface of bacteria targeted for autophagy.[13,14] NBR1 also has the distinctive "J" domain[12] that allows it to anchor to membranes, and that is also essential for normal pexophagy. The combination of self-interaction, domains, and membrane anchoring suggests that NBR1 could exhibit biological coarsening dynamics. Since a threshold number of NBR1 appears to be required on a peroxisome to trigger pexophagy,[12] coarsening could then be a mechanism to concentrate receptor proteins on particular organelles and so select them for degradation.

In order to understand how the physics of coarsening might influence biological processes such as autophagy substrate specificity, we model the coarsening of surface clusters on a polydisperse collection of spherical drops. There has been little study of coarsening on such a collection of disconnected objects, though coarsening is well understood in bulk systems. For well-separated bulk clusters, coarsening is driven by Ostwald ripening at late times – where material evaporates from clusters smaller than the critical radius r_c and condenses onto clusters larger than r_c.[15,16] The key features are a growing critical cluster size,[17,18] with $r_c(t) \sim t^{1/3}$, and dynamic scaling[1] of cluster size distributions with respect to $r_c(t)$. While scaling distributions vary with spatial dimension,[1,15,17,19] the universal dynamical exponent 1/3 does not.[1]

Department of Physics and Atmospheric Science, Dalhousie University, Halifax, NS, Canada B3H 4R2. E-mail: andrew.rutenberg@dal.ca

We work in the dilute limit of Lifshitz–Slyozov–Wagner (LSW),[1,17,18] with a uniform bulk concentration[1,17] of molecules $\rho(t)$ that couples clusters on different drops. A uniform bulk concentration is a good approximation when cluster separation is larger than cluster size.[1,15,17] Our investigation considers three questions. First, in what way is canonical coarsening changed by having surface clusters on drops rather than bulk clusters in space? Second, how do the details of drop polydispersity, *i.e.* the drop size distribution, affect coarsening behaviour? Third, what aspects of this system could affect biological behaviour – in particular autophagy selectivity? We aim to understand the physical behaviour of idealized coarsening clusters on drops, and identify how the qualitative characteristics of this process could play a role in protein cluster selection of substrates for autophagy.

2 Model

The growth and evaporation of coarsening clusters on drops will be determined by the vapour phase surrounding the clusters on the drop surface. Accordingly, we first consider the dynamics of a dilute concentration field of molecules, $f(\theta,\phi,t)$, on the surface of a single spherical drop of radius R, coupled to the bulk by association and dissociation from the drop surface:

$$\frac{\partial f}{\partial t} = D_s \nabla^2 f + \frac{\rho(t)D_b}{R} - \frac{\Gamma_{off}}{R}f. \qquad (1)$$

The first term on the right is surface diffusion, with diffusivity D_s. The second term is diffusion-limited molecule association with the surface, proportional to a time-dependent bulk molecule concentration ρ and the bulk diffusivity D_b, and inversely proportional to the drop radius R due to diffusion-limited association.[20] Note that the total diffusive flux of molecules associating with the entire sphere surface is thus $4\pi\rho(t)D_b R$. The third term is molecule dissociation from the surface, proportional to the parameter Γ_{off} and molecule concentration f, and inversely proportional to the drop radius R – see Appendix A for development of this term. In steady state ($\partial f/\partial t = 0$), a uniform surface density is then independent of drop radius, with $f_{ss} = \rho(t)D_b/\Gamma_{off}$.

The molecule flux to the perimeter of a circular cluster of molecules on the sphere surface will be determined by the concentration field. There will not be a cluster on all spheres at all times since below a critical surface concentration clusters will be unstable to evaporation. Above this threshold concentration, clusters will nucleate and grow. Clusters in small biological systems, such as holin domains in bacteria[3,21] and polarity clusters in yeast,[22] often nucleate and coalesce rapidly. Similarly, we assume that nucleated clusters have resolved into (at most) a single circular cluster per drop.

To determine the growth of a cluster of N particles subtending a polar angle θ_c on a spherical drop of radius R (see Fig. 1), the concentration field f must be found. In steady state, eqn (1) can be rewritten as a general Legendre equation and solved.[23,24] (This solution, and subsequent development are shown in more detail in Appendix B.) We apply the Gibbs–Thomson boundary condition at the perimeter of the circular cluster, at
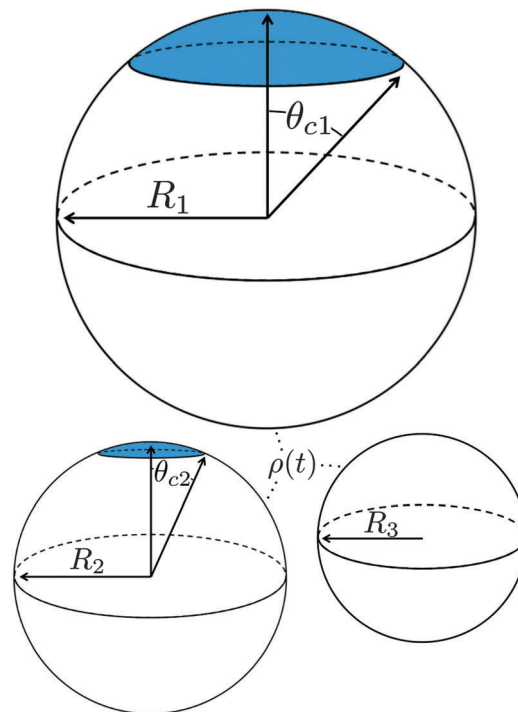

Fig. 1 Illustration of our model geometry, not to scale, using three spherical drops. Drops 1 and 2 have clusters (symbolized by the circular blue cap) and drop 3 does not have a cluster. Drops may have different radii (R_i), and any clusters subtend a polar angle θ_{ci}. Molecules on the surface of each drop exchange material with the bulk concentration $\rho(t)$.

θ_c, $f(\theta)|_{\theta=\pi-\theta_c} = f_\infty\left(1 + \frac{\nu}{R\sin\theta_c}\right)$, with f_∞ the concentration at a flat interface and ν the capillary length, which determines the decay length of the number density at the edge of the cluster and that we assume to be small.[15,25–27] This gives us $f(\theta) = CP_\lambda(\cos\theta) + D_b\rho/\Gamma_{off}$, with the limiting form of the hypergeometric function of index λ $P_\lambda(x) = \frac{\sin(\lambda\pi)}{\pi}\left[\ln\left(\frac{1+x}{2}\right) + \gamma + 2\psi(\lambda+1) + \pi\cot(\lambda\pi)\right]$,[24] γ the Euler–Mascheroni constant, ψ the digamma function, $\lambda = -\frac{1}{2}\pm\frac{1}{2}\sqrt{1-4a}$, and $a \equiv \Gamma_{off}R/D_s$. The coefficient C is given by

$$C \equiv \frac{f_\infty(1+\nu/(R\sin\theta_c)) - D_b\rho/\Gamma_{off}}{(\sin(\lambda\pi)/\pi)\left[\log\left(\frac{1}{2}-\frac{1}{2}\cos\theta_c\right) + \gamma + 2\psi(\lambda+1) + \pi\cot(\lambda\pi)\right]}. \qquad (2)$$

Mass balance with the diffusive flux of molecules to the cluster edge then determines the change in cluster size with time:

$$\frac{d\theta_c}{dt} = \frac{CD_s b\sin(\lambda\pi)}{\pi R^2}\frac{\sin\theta_c}{1-\cos\theta_c}, \qquad (3)$$

where b is the area per molecule in a surface cluster.

The denominator of C has a logarithmic term, as seen in two-dimensional coarsening.[1,15,19] For fast diffusive equilibration compared to molecule number equilibration, $a = \Gamma_{off}R/D_s \ll 1$,

and a small cluster $\theta_c \ll 1$, the denominator of C is dominated by the $\cot(\lambda\pi) \simeq \cot(-a\pi) \simeq -1/a$ term. Using this approximation, dependence on the surface diffusivity D_s is cancelled, and we can express the result in terms of the number of molecules N in the cluster for small θ_c,

$$\frac{dN}{dt} \simeq 4\pi R \left(D_b \rho(t) - f_\infty \Gamma_{off} \left(1 + \nu \sqrt{\frac{\pi}{bN}} \right) \right). \quad (4)$$

This is similar in form to typical $d = 3$ descriptions of cluster dynamics.[1,15]

We investigate ensembles of many drops using two qualitatively-distinct radius distributions $P_0(R)$ with the same mean $\bar{R}$: one with and the other without a continuous tail. A uniform distribution has no tail, with $R \in [\bar{R} - R_0, \bar{R} + R_0]$, and $P_0(R) = 1/(2R_0)$. The exponential distribution has a tail, with $R \in [R_{min}, \infty)$, $P_0(R) = R_0^{-1} e^{-(R-R_{min})/R_0}$, and $R_{min} = \bar{R} - R_0$. We choose $\bar{R} = 0.25$ μm to be consistent with peroxisome sizes.[28]

To obtain a simplified dynamical equation for number of particles N_i in the cluster on the ith drop, we define $\alpha \equiv 4\pi D_b/\bar{R}^2$, a corresponding dimensionless time $t' \equiv \alpha t$, the bulk density corresponding to surface saturation $\rho_c \equiv f_\infty \Gamma_{off}/D_b$, and the corresponding bulk supersaturation $\Delta\rho \equiv \rho(t) - \rho_c$, so that

$$\frac{dN_i(t')}{dt'} = \bar{R}^2 R_i \left[\Delta\rho - \frac{\beta}{\sqrt{N}} \right], \quad (5)$$

where we also conserve molecular numbers, so that $d\Delta\rho/dt' = -\langle dN_i/dt' \rangle / L^3$ where L^3 is the bulk cellular volume per drop. The parameter $\beta \equiv \sqrt{\pi} \Gamma_{off} f_\infty \nu / (D_b \sqrt{b})$ characterizes the effect of cluster curvature through the supersaturation necessary to avoid evaporation of finite-size surface clusters.

What is the expected scale of β? Capillary lengths of approximately one[26] and several[27] particle widths have been found for 2d and 3d systems, respectively. Assuming that the capillary length is approximately the size of a cluster molecule, $\nu/\sqrt{b} \simeq 1$, then $\beta \simeq \sqrt{\pi} \Gamma_{off} f_\infty / D_b$. A typical cytosolic protein diffusivity[28] is $D_b \simeq 1$ μm^2 s^{-1}, and an approximate lower-bound for f_∞ is determined by a single molecule per sphere, i.e. $f_\infty \gtrsim 1/(4\pi\bar{R}^2) \simeq 1$ μm^{-2}. The timescale for number equilibration on the drop surface is $\bar{R}/\Gamma_{off}$. We choose as our default value $\beta = 0.01$ μm^{-3}, corresponding to equilibration in tens of seconds, and explore the effects of varying β below. We note that for a typical cellular volume $V = 5000$ μm^3, this choice of β corresponds to supersaturation by only 50 cytosolic molecules. Larger capillary lengths, $\nu/\sqrt{b} > 1$, require larger surface number equilibration times to achieve the same β.

To get better statistics, 10^7 drops are used for each simulation, all of which initially have clusters, and results are also averaged over 100 sets of initial conditions, unless otherwise stated. The initial supersaturation $\Delta\rho(0) = \Delta\rho_0$, and cluster sizes are initially proportional to their drop surface area, $N_i(0) = N_0 (R_i/\bar{R})^2$. Other initial conditions, such as equal cluster sizes or cluster sizes randomly drawn from a uniform distribution, give qualitatively similar results at late times. Unless otherwise stated, $\Delta\rho_0 = 0.1$ μm^{-3}, and $N_0 = 50$ – variation of these

parameters is explored below. Our bulk volume is $L^3 = 100$ μm^3 per drop, so that the initial available bulk number of molecules is $\Delta\rho_0 L^3 = 10$ per drop. For stable numerical results at early times timesteps must be small, but can be larger at later times.[29] We use a timestep $\Delta t' = 10(10t')^{1/3}$ until $\Delta t' = 10^5$, after which $\Delta t'$ is held constant.

3 Results

The critical cluster size $r_c(t)$ is an important quantity for LSW coarsening – we measure the average number of molecules in a cluster, $\langle N \rangle$, where $\langle N \rangle \sim r_c^2$. By numerically evolving eqn (5) we confirmed that the average cluster size follows the LSW[1,17] power-law $\langle N \rangle \sim t^{2/3}$ at later times, as shown in the insets of Fig. 2(a) and (c). Fig. 2 shows the cluster size distributions for uniform and exponential drop radius distributions. The cluster size distributions exhibit good dynamical scaling for at least three decades in time. The power-law growth and scaling was seen for all tested initial conditions, as well as for a range of two decades variation of β, the initial bulk supersaturation $\Delta\rho_0$, and the initial cluster size N_0 values.

However, Fig. 3 illustrates how the scaling function depends on the type of drop radius distribution. The scaled distribution is distinctly different for uniform vs. exponential drop radius distributions. For the uniform drop radius distribution, there is no dependence on the distribution width parameter, R_0. For the exponential drop radius distribution, the scaled cluster size distributions depend on the width parameter R_0, becoming sharper as R_0 decreases. We also show two analytic solutions for scaling distributions of bulk clusters in 2d (dashed black line)[19]
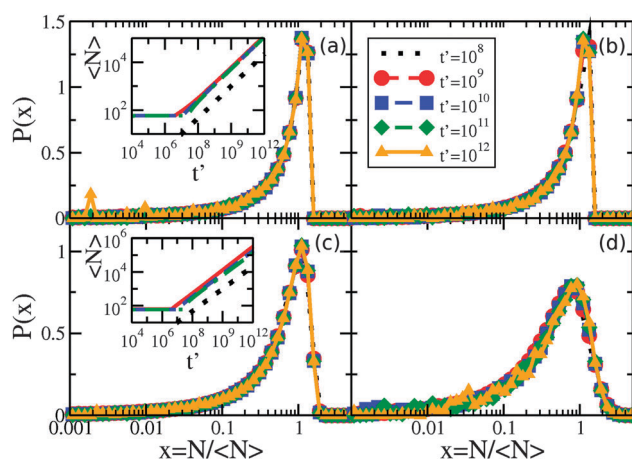
Fig. 2 Scaling of the cluster size distribution for the times indicated by the legend in panel (b): (a) linear-log plot of $P(N/\langle N \rangle)$ vs. $N/\langle N \rangle$ for a narrow uniform drop radius distribution with $R_0 = 0.001$ μm, (b) wide uniform drop radius distribution with $R_0 = 0.05$ μm, (c) narrow exponential drop radius distribution with $R_0 = 0.001$ μm, and (d) wide exponential drop radius distribution with $R_0 = 0.05$ μm. Inset of (a) shows the average cluster size in time for uniform drop radius distributions with $R_0 = 0.05$ μm (solid red line), $R_0 = 0.01$ μm (dashed blue), and $R_0 = 0.001$ μm (dashed-dotted green), along with the expected $t^{2/3}$ growth law indicated by the dotted black line. Inset of (c) is similar, with exponential drop radius distributions with $R_0 = 0.05$ μm (solid red line), $R_0 = 0.01$ μm (dashed blue), and $R_0 = 0.001$ μm (dashed-dotted green).
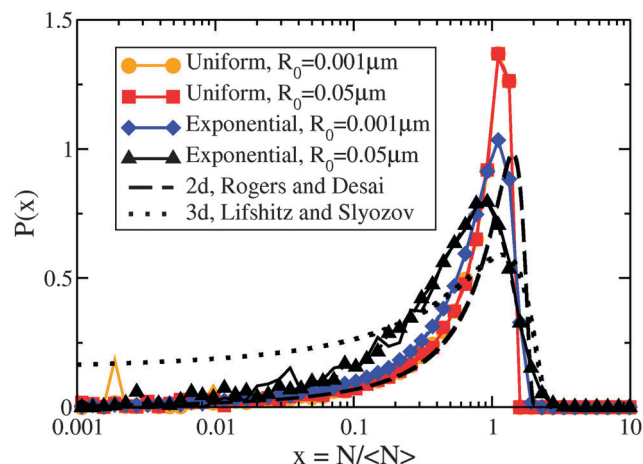
**Fig. 3** Non-universal cluster size distributions. Linear-log plot of cluster-size distributions $P(N/\langle N \rangle)$ vs. $N/\langle N \rangle$ for several drop radius distributions as indicated in the legend. Two times, $t' = 10^{11}$ and 10^{12}, are shown overlapping for each condition with dashed and solid coloured lines, respectively. Although each drop radius distribution exhibits scaling collapse, the different types of drop radius distributions do not collapse to the same scaling function. All uniform sphere radius distributions collapse to the same scaling function, while the exponential sphere radius distributions collapse to functions that vary with the drop distribution width. The black lines show analytic scaling distributions from the literature[17,19] for $d = 2$ and $d = 3$, both in the dilute limit.

and 3d (dotted black line).[17] The scaling distributions for clusters on drops are qualitatively similar to the 2d distribution, rapidly approaching zero as the cluster size $N \rightarrow 0$. Near the peak, the effect on the scaling function of changing the form of the drop size distribution is similar in magnitude to the effect of changing the spatial dimension between 2d and 3d for bulk coarsening.

At later times only the larger drops retain clusters – a phenomenon we call size-mediated cluster selectivity. Fig. 4(a) and (b) show the radius of the smallest drop with a cluster, $R_{\min}$. With increasing times, $R_{\min}$ suddenly increases at a characteristic onset time. This t_{onset} coincides with the beginning of the power-law coarsening regime shown in the insets of Fig. 2, after which dynamical scaling collapse of cluster size distributions is observed. Further, by considering the size distribution of drops that retain clusters, as shown in Fig. 5, we see that the smallest of the drops still retaining clusters are always next to lose their clusters. The distribution of larger drops with clusters remains unchanged, indicating larger drops do not lose their clusters until all smaller drops have done so.

As seen in Fig. 4(c), the timing of t_{onset} is controlled by β, $\Delta\rho_0$, N_0, and R_0. Both $\Delta\rho_0$ and N_0 would be directly affected by protein expression rates: $\Delta\rho_0$ is related to the initial bulk concentration of proteins, and represents how much protein remains in the bulk once clusters have nucleated on drops, while N_0 represents the number of proteins initially present in each cluster. While β, which is proportional to how quickly a protein dissociates from a membrane, may not be easily controlled, we do expect it to vary *in vivo* due to differences in membrane lipid composition,[30,31] such as between organelles. The width of the drop size distribution, R_0, is related to the
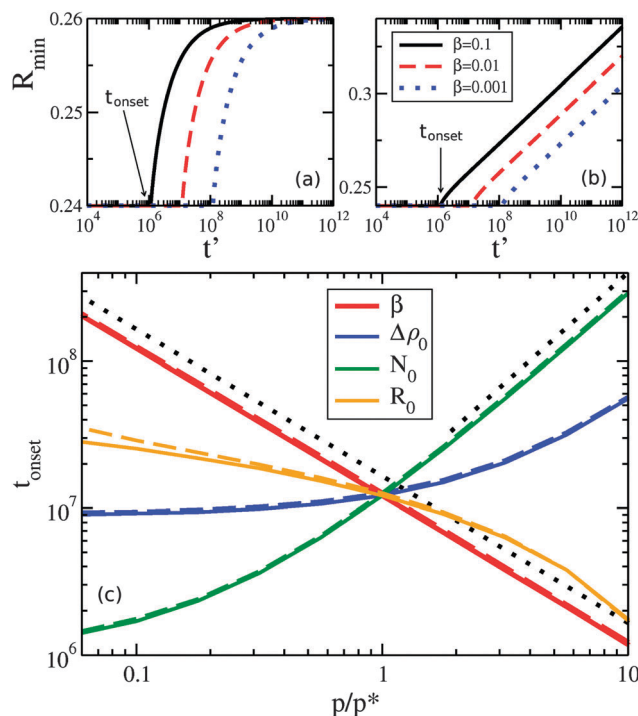
Fig. 4 Minimum drop size with clusters $R_{\min}$ vs. time t' for (a) uniform and (b) exponential drop size distributions. In (a) and (b) we vary β as shown and hold other parameters at default values. The abrupt increase of $R_{\min}$ defines a time t_{onset}, shown by arrows for the $\beta = 0.1$ μm^{-3} curves. In (c), t_{onset} is shown as various parameters p [where p equals each of β (thicker, red), initial bulk supersaturation $\Delta\rho_0$ (darker, blue), initial cluster size N_0 (green), or drop-size distribution width R_0 (orange)] are varied with respect to their default values $p^\star$. We use $p^\star = 0.01$ μm^{-3}, 0.1 μm^{-3}, 50, and 0.01 μm for β, $\Delta\rho_0$, N_0, and R_0, respectively, and average over 10 sets of random initial conditions. Solid and dashed curves show results for uniform and exponential drop size distributions, respectively. The black dotted lines indicate expected asymptotic power law behaviour with exponents −1 and 1.5, following the β or N_0 data, respectively.
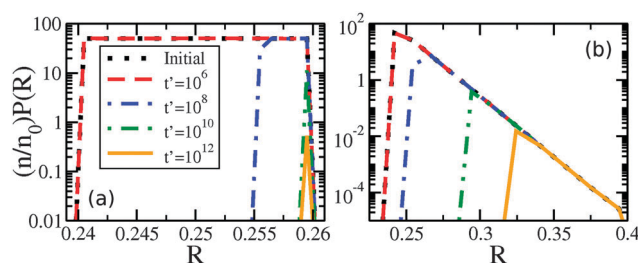
Fig. 5 Number density of drop radii with clusters remaining, $(n/n_0)P(R)$, vs. R for (a) uniform drop radius distribution with $R_0 = 0.01$ μm and (b) exponential drop radius distribution with $R_0 = 0.01$ μm. The times indicated by the legend in (a) apply to both panels, and the default parameters are used in both cases. We note that n is the number of spheres with clusters remaining, n_0 the initial number, and $P(R)$ is the drop size distribution.

amount and magnitude of organelle size variation, which could vary with conditions or cell type. We note that changing the initial cluster size distribution, so that instead of clusters proportional to drop area we used either equal or uniformly random cluster sizes, delayed t_{onset}.

We can qualitatively understand some of the asymptotic behavior shown in Fig. 4(c). For example, $t_{onset} \sim 1/\beta$ reflects the β dependence of the evaporative term in eqn (5) – indicating that cluster evaporation largely determines t_{onset}. Consistent with this, at larger values of N_0 we see that $t_{onset} \sim N_0^{1.5}$. The cluster size-dependent term in eqn (5) is $dN/dt \sim -N^{-0.5}$, which gives an evaporation time $\sim N_0^{1.5}$ for a cluster of initial size N_0. The dependence on the initial bulk density $\Delta\rho_0$ is similar to N_0. At smaller values of $\Delta\rho_0$ (at fixed N_0) we see that t_{onset} approaches a constant value. This occurs when the material in the initial clusters dominates the bulk density, and a similar cross-over is seen with smaller values of N_0 at fixed $\Delta\rho_0$. Increasing R_0 decreases t_{onset}, as drop size differences drive the migration of material.

4 Discussion

Coarsening of clusters on drops exhibits LSW-like power law cluster growth[1] and dynamic scaling, as shown in Fig. 2. Scaling distributions typically depend on both spatial dimension and volume fraction,[1] but are also known to depend on some aspects of the evolution equations such as spatial anisotropy.[32] In this paper we have shown that the scaling cluster-size distribution depends on the shape of the drop radius distribution, and can also depend on its width. Distinct distributions are seen with uniform vs. exponential drop-size distributions. We expect that drop-size distributions with compact support (e.g. the uniform distribution) will have the same cluster size scaling functions as the uniform distribution, while drop-size distributions with tails (e.g. power laws) may have scaling functions that vary with the drop-size distribution width. Power law growth, scaling collapse, and similar t_{onset} behaviour are seen for both the uniform distribution, which has no tail at large drop sizes, and the exponential distribution, which does have a tail. At late times the remaining clusters are on large drops. Given the similarity of behaviour between uniform and exponential drop-size distributions, we expect similar behaviour independent of the details of the distribution. Both peroxisome[33,34] and vesicle[35] size distributions are qualitatively similar to our exponential distribution, with a continuously decreasing tail at large sizes.

We have demonstrated that at later times larger drops are selected to retain clusters, while smaller drops have no clusters. The start of size-based selectivity is sudden, and described by the time t_{onset} that approximately coincides with the onset of dynamical scaling in these systems. Once selectivity has begun, and as coarsening progresses, the clusters on the smallest occupied drops progressively evaporate while clusters on larger drops will grow.

The autophagy receptor protein NBR1 is able to both self-interact and bind to membranes, and is a receptor protein for peroxisome autophagy, i.e. pexophagy.[12] In line with our results, we propose that NBR1 clusters on small peroxisomes will evaporate, while those on larger peroxisomes will grow. As NBR1 clusters on small peroxisomes shrink and evaporate, and those on larger peroxisomes grow, the NBR1 cluster growth on larger peroxisomes would push these peroxisomes over any threshold number of NBR1 for autophagy.[12] This would be a

physical mechanism leading to the selective degradation of larger organelles by autophagy, on the basis of size.

Our proposed mechanism of size-selection through receptor cluster coarsening is consistent with the observation of receptor protein clusters.[13,14] It is also consistent with the observation by Deosaran et al.[12] who show (see Fig. 5) significant colocalization of NBR1 and peroxisomes (indicated by catalase), but with an all-or-none character. Catalase spots either colocalize with significant amounts of NBR1 or background levels. Indeed, our model shows that significantly higher NBR1 levels on drops with clusters than without – and only some drops supporting clusters at later times. Finally, our mechanism could also explain the observation that, in situations inducing a reduction in peroxisome number, larger peroxisomes degrade earlier and preferentially relative to smaller peroxisomes.[10] Degradation also depends upon peroxisome size in yeast.[11]

How does the timing of our cluster selectivity correspond to that of peroxisome autophagy? In Fig. 4, our default values of β, $\Delta\rho_0$, N_0, and R_0 result in $t_{onset} \sim 10^7$. Using $t = t'/\alpha$, $D_b = 1\ \mu m^2$ as a typical cytosolic diffusivity, so that $\alpha = 4\pi D_b/\bar{R}^2 \simeq 200\ s^{-1}$, the onset of cluster selectivity is as early as $t \sim 10^4$–10^5 seconds. This timescale is consistent with mammalian autophagy, which occurs in days.[36,37] Individual variation of β and N_0, shown in Fig. 4(c), can push t_{onset} down to 10^6, and combined variation (data not shown) can push t_{onset} even earlier – these timescales are consistent with peroxisome autophagy in yeast, which occurs in hours.[38,39] Therefore the segregation of clusters to larger organelles through coarsening, as proposed here, can be fast enough to play a significant role in the selective degradation of larger peroxisomes.

Fig. 4 shows how the parameters β, $\Delta\rho_0$, N_0, and R_0 can vary the timing of cluster selectivity, t_{onset}. Increasing either the initial bulk supersaturation $\Delta\rho_0$ or the initial cluster size parameter N_0, i.e. expressing more clustering proteins, has the counterintuitive effect of delaying size selectivity. This suggests that experimentally adjusting expression of receptor proteins such as NBR1 would have a significant effect on the speed of autophagy response, with moderately larger expression potentially delaying autophagy. A decreased off-rate of receptor (through Γ_{off} and hence β) also leads to delayed size-selectivity. Larger numbers or more tightly bound receptors both lead to slower size-selectivity for our physical coarsening mechanism, since it depends upon the loss of receptors from smaller clusters. Conversely, increasing variation in drop size, represented by R_0, leads to earlier size-selectivity.

We have explored a physical mechanism of size-selection exploiting cluster coarsening on drops. We were motivated by how this may provide a physical basis for autophagy substrate selectivity in pexophagy. A similar cluster-coarsening mechanism may allow PEX11, a protein important to the division of peroxisomes that self-interacts and sticks to membranes,[40] to target larger peroxisomes. Similarly, SNARE proteins are required to facilitate vesicle fusion[41] and are thought to form membrane clusters. A similar selective coarsening mechanism could thereby select larger vesicles for fusion. Nevertheless, we expect that in vivo other biological processes will also be

involved and could modify cluster formation or selectivity. For example, ubiquitin is thought to play a role in recruiting NBR1 to peroxisome membranes,[12] and a low peroxisome ubiquitin level[28] or other signals or interactions may prevent NBR1 from forming clusters and selecting peroxisomes for autophagy. In addition, different types of autophagy receptors often interact.[6,7] We have started with the properties of only one receptor, modelled after NBR1. Another receptor, p62, interacts with NBR1[42] and enhances pexophagy.[12] It will be interesting to consider how interactions with p62 may modify the selectivity mechanism we have proposed here.

5 Conclusion

We model the coarsening behaviour of clusters of molecules on the surface of spherical drops. We determine the dynamical equation for cluster size and, using an ensemble of polydisperse drops, recover the Lifshitz–Slyozov–Wagner exponent for cluster growth and dynamical scaling. The cluster-size scaling function is found to depend on the drop-size distribution, which affects the scaling function to a similar degree as spatial dimension does in bulk systems. Among remaining clusters, evaporation occurs from smaller drops first, with clusters on larger drops growing. This selection of larger drops by clusters may be significant to the cell-biological process of autophagy. Autophagy receptor proteins are seen to cluster, and the receptor protein NBR1 is sufficient for peroxisome autophagy and has domains suggesting it clusters and associates with membranes. Our observation of the selection of larger drops by clusters suggests that clustering NBR1 proteins on peroxisome surfaces could similarly select larger peroxisomes for NBR1 clusters, thereby selecting these larger peroxisomes for degradation by autophagy. This presents a possible physical mechanism to explain reported size selection during peroxisome degradation by autophagy.

Appendix A

Eqn (1) describes the change in molecule concentration f on the surface of a sphere of radius R due to diffusion-limited association of molecules from the bulk and dissociation of molecules from the sphere surface. The dissociation term is $-\Gamma_{off}f/R$, and is controlled by the Γ_{off} parameter.

Successful dissociation includes diffusive escape from the immediate surface. The probability of recapture[20] by an absorbing sphere of radius R for a diffusive molecule initially at radial distance r is $P_{capture} = R/r$. The probability of escape is then $P_{escape} = 1 - R/r$. A molecule initially immediately adjacent to the sphere surface will be at distance $r = R + b$ for a molecule of radius b, and for $b \ll R$,

$$P_{escape} = 1 - \frac{R}{R+b} = 1 - (1 + b/R)^{-1} \simeq 1 - (1 - b/R)$$
$$= b/R. \tag{6}$$

We expect that isolated NBR1 molecules will locally unbind from the membrane at a constant rate, independent of the small membrane curvature. However effective escape will be controlled by eqn (6), since most molecules will immediately rebind. The overall

dissociation rate will therefore be proportional to R^{-1}. All dependence on molecule radius, unbinding (and recapture) of anchoring domains such as the NBR1 'J' domain, and other factors will then be contained in the Γ_{off} parameter. Since diffusion limited association has the same R dependence, this results in an R independent surface concentration in steady state.

Appendix B

This appendix follows the development of a dynamical equation for cluster size on a sphere, eqn (5), starting with eqn (1)

$$\frac{\partial f}{\partial t} = D_s \nabla^2 f + \frac{\rho(t)D_b}{R} - \frac{\Gamma_{off}}{R}f, \tag{7}$$

where f is the concentration field, D_s is the surface diffusivity, ρ is the bulk molecule concentration, D_b is the bulk diffusivity, Γ_{off} is the dissociation parameter, and R is the sphere radius. We transform to $\tilde{f} = f - \rho D_b/\Gamma_{off}$, define $\tilde{a} = \Gamma_{off}/R$, go to steady state ($\partial f/\partial t = 0$), and only keep the θ dependence of the Laplacian due to assumed azimuthal symmetry for a polar cluster:

$$\tilde{a}\tilde{f} = D_s \nabla^2 \tilde{f} = \frac{D}{R^2 \sin\theta}\frac{\partial}{\partial\theta}\left(\sin\theta\frac{\partial\tilde{f}}{\partial\theta}\right). \tag{8}$$

We now set $x = \cos\theta$ and $a = \tilde{a}R^2/D_s$ to give us

$$(1 - x^2)\frac{\partial^2\tilde{f}}{\partial x^2} - 2x\frac{\partial\tilde{f}}{\partial x} - a\tilde{f} = 0, \tag{9}$$

which is a hypergeometric differential equation.[23] Only f near the polar cluster is needed to determine cluster dynamics, and so we use the limiting form[24] of the solution as $x \to -1$, or equivalently as $\theta \to \pi$

$$P_\lambda(x) = \frac{\sin(\lambda\pi)}{\pi}\left[\ln\left(\frac{1+x}{2}\right) + \gamma + 2\psi(\lambda + 1) + \pi\cot(\lambda\pi)\right], \tag{10}$$

where $\lambda = -\frac{1}{2} \pm \frac{1}{2}\sqrt{1 - 4a}$, γ is the Euler–Mascheroni constant, and ψ is the digamma function. So our solution for $\tilde{f}$ is then $\tilde{f} = CP_\lambda(\cos\theta)$, or

$$f = CP_\lambda(\cos\theta) + \rho D_b/\Gamma_{off}. \tag{11}$$

The Gibbs–Thomson boundary condition[15,25–27] determines the elevated vapour pressure in equilibrium with a curved interface. We apply this condition at the perimeter of our circular cluster on the pole of the sphere, which covers an angle θ_c from the pole:

$$f(\theta)|_{\theta=\pi-\theta_c} = f_\infty\left(1 + \frac{\nu}{R\sin\theta_c}\right). \tag{12}$$

Applying this condition to eqn (11) gives

$$C \equiv \frac{f_\infty(1 + \nu/(R\sin\theta_c)) - D_b\rho/\Gamma_{off}}{(\sin(\lambda\pi)/\pi)\left[\log\left(\frac{1}{2} - \frac{1}{2}\cos\theta_c\right) + \gamma + 2\psi(\lambda + 1) + \pi\cot(\lambda\pi)\right]}, \tag{13}$$

where the Euler–Mascheroni constant $\gamma \simeq 0.577$.

Now we apply mass balance, determining the change in cluster area by the diffusive flux of molecules to the cluster perimeter:

$$\frac{d}{dt}\left[2\pi R^2(1-\cos\theta_c)\right] = \left[2\pi R\sin\theta_c D_s\frac{\partial f}{\partial(-R\theta)}\bigg|_{\theta=\pi-\theta_c}\right]b, \quad (14)$$

where b is the area per molecule. Inserting eqn (12) into eqn (14) gives

$$\frac{d\theta_c}{dt} = \frac{CD_s b\sin(\lambda\pi)}{\pi R^2}\frac{\sin\theta_c}{1-\cos\theta_c}. \quad (15)$$

For $\theta_c \ll 1$ we have $\sin\theta_c \simeq \theta_c$, and $\cos\theta_c \simeq 1 - \theta_c^2/2$. Putting these into the expression for C gives us

$$\frac{d\theta_c}{dt} = \frac{2D_s b[D_b\rho/\Gamma_{off} - f_\infty(1+\nu/(R\theta_c))]}{R^2\theta_c[\log(\theta_c^2/4)+\gamma+2\psi(\lambda+1)+\pi\cot(\lambda\pi)]}. \quad (16)$$

The denominator of the right side of this equation has four terms, with the relative size determined by $\theta_c \ll 1$, and $a \ll 1$, which leads to $\lambda \simeq -a$. For the digamma function, $\psi(\lambda+1) \simeq \psi(-a+1) \simeq \psi(1) = -\gamma$, while $\cot(\lambda\pi) \simeq \cot(-a\pi) \simeq -1/(a\pi)$. We assume that $|\ln(\theta_c^2/4)| \ll 1/a$, which is equivalent to $\theta_c^2 \gg e^{-1/a}$, which is expected to be the case for $a \ll 1$. This implies that $\pi\cot(\lambda\pi) \simeq -1/a$ is the dominant term of the denominator, and that

$$\frac{d\theta_c}{dt} \simeq \frac{2D_s ba[D_b\rho/\Gamma_{off} - f_\infty(1+\nu/(R\theta_c))]}{R^2\theta_c}$$

$$= \frac{2b\Gamma_{off}[D_b\rho/\Gamma_{off} - f_\infty(1+\nu/(R\theta_c))]}{R\theta_c}. \quad (17)$$

Assuming θ_c is small, $bN = \pi(R\theta_c)^2$, we have $d\theta_c/dt = 1/(2R)\sqrt{b/(\pi N)}\,dN/dt$ and so

$$\frac{dN}{dt} = 4\pi R\left[D_b\rho - \Gamma_{off}f_\infty\left(1+\frac{\nu}{R\theta_c}\right)\right]. \quad (18)$$

We define a mean sphere radius $\bar{R}$, $\alpha = 4\pi D_b/\bar{R}^2$, a dimensionless time $t' = \alpha t$, and bulk density corresponding to surface saturation $\rho_c = f_\infty\Gamma_{off}/D_b$, and a bulk supersaturation $\Delta\rho = \rho(t) - \rho_c$. This then gives us

$$\frac{1}{(4\pi D_b/\bar{R}^2)}\frac{dN}{dt} = R\bar{R}^2\left[\rho(t)-\frac{f_\infty\Gamma_{off}}{D_b}-\frac{\sqrt{\pi}\Gamma_{off}f_\infty\nu}{D_b\sqrt{b}}\frac{1}{\sqrt{N}}\right], \text{ or}$$

$$\frac{dN}{dt'} = R\bar{R}^2\left(\Delta\rho - \frac{\beta}{\sqrt{N}}\right). \quad (19)$$

Acknowledgements

References

1 A. J. Bray, *Adv. Phys.*, 2002, **51**, 481–587.
2 J. Derr and A. D. Rutenberg, *Phys. Rev. E: Stat., Nonlinear, Soft Matter Phys.*, 2011, **84**, 011928.
3 G. L. Ryan and A. D. Rutenberg, *J. Bacteriol.*, 2007, **189**, 4749–4755.
4 M. Semplice, A. Veglio, G. Naldi, G. Serini and A. Gamba, *PLoS One*, 2012, 7, e30977.
5 A. Stolz, A. Ernst and I. Dikic, *Nat. Cell Biol.*, 2014, **16**, 495–501.
6 G. M. Fimia, G. Kroemer and M. Piacentini, *Cell Death Differ.*, 2013, **20**, 1–2.
7 V. Rogov, V. Dotsch, T. Johansen and V. Kirkin, *Mol. Cell*, 2014, **53**, 167–178.
8 J. Ezaki, E. Kominami and T. Ueno, *IUBMB Life*, 2011, **63**, 1001–1008.
9 S. J. Huybrechts, P. P. van Veldhoven, C. Brees, G. P. Mannaerts, G. V. Los and M. Fransen, *Traffic*, 2009, **10**, 1722–1733.
10 M. Veenhuis, K. Zwart and W. Harder, *FEMS Microbiol. Lett.*, 1978, **3**, 21–28.
11 T. Y. Nazarko, J.-C. Farre and S. Subramani, *Mol. Biol. Cell*, 2009, **20**, 3828–3839.
12 E. Deosaran, K. B. Larsen, R. Hua, G. Sargent, Y. Wang, S. Kim, T. Lamark, M. Jauregui, K. Law, J. Lippincott-Schwartz, A. Brech, T. Johansen and P. K. Kim, *J. Cell Sci.*, 2013, **126**, 939–952.
13 M. Cemma, P. K. Kim and J. H. Brumell, *Autophagy*, 2011, **7**, 341–345.
14 P. Wild, H. Farhan, D. G. McEwan, S. Wagner, V. V. Rogov, N. R. Brady, B. Richter, J. Korac, O. Waidmann, C. Choudhary, V. Dotsch and D. Bumann and I. Dikic, *Science*, 2011, **333**, 228–233.
15 J. H. Yao, K. R. Elder, H. Guo and M. Grant, *Phys. Rev. B: Condens. Matter Mater. Phys.*, 1993, **47**, 110–125.
16 P. W. Voorhees, *J. Stat. Phys.*, 1985, **38**, 231–252.
17 I. M. Lifshitz and V. V. Slyozov, *J. Phys. Chem. Solids*, 1961, **19**, 35–50.
18 C. Wagner, *Z. Elektrochem.*, 1961, **65**, 581–591.
19 T. M. Rogers and R. C. Desai, *Phys. Rev. B: Condens. Matter Mater. Phys.*, 1989, **39**, 956–964.
20 H. C. Berg and E. M. Purcell, *Biophys. J.*, 1977, **20**, 193–219.
21 R. White, S. Chiba, T. Pang, J. S. Dewey, C. G. Savva, A. Holzenburg, K. Pogliano and R. Young, *Proc. Natl. Acad. Sci. U. S. A.*, 2011, **108**, 798–803.
22 A. S. Howell, M. Jin, C.-F. Wu, T. R. Zyla, T. C. Elston and D. J. Lew, *Cell*, 2012, **149**, 322–333.
23 I. A. Stegun, Legendre functions, in *Handbook of mathematical functions*, ed. M. Abramowitz, I. A. Stegun, National Bureau of Standards, 1970.
24 A. Erdelyi, W. Magnus, F. Oberhettinger and F. G. Tricomi, *Higher Transcendental Functions*, McGraw-Hill, 1953, vol. 1.
25 D. O. Yi, M. H. Jhon, I. D. Sharp, Q. Xu, C. W. Yuan, C. Y. Liao, J. W. Ager III, E. E. Haller and D. C. Chrzan, *Phys. Rev. B: Condens. Matter Mater. Phys.*, 2008, **78**, 245415.

26 B. Krishnamachari, J. McLean, B. Cooper and J. Sethna, *Phys. Rev. B: Condens. Matter Mater. Phys.*, 1996, **54**, 8899–8907.

27 M. Strobel, K.-H. Heinig and W. Moller, *Phys. Rev. B: Condens. Matter Mater. Phys.*, 2001, **64**, 245422.

28 A. I. Brown, P. K. Kim and A. D. Rutenberg, *PLoS Comput. Biol.*, 2014, **10**, e1003426.

29 B. P. Vollmayr-Lee and A. D. Rutenberg, *Phys. Rev. E: Stat., Nonlinear, Soft Matter Phys.*, 2003, **68**, 066703.

30 I. Ispolatov and A. Musch, *PLoS Comput. Biol.*, 2013, **9**, e1003125.

31 C. C. Hayden, J. S. Hwang, E. A. Abate, M. S. Kent and D. Y. Sasaki, *J. Am. Chem. Soc.*, 2009, **131**, 8728–8729.

32 A. D. Rutenberg and B. P. Vollmayr-Lee, *Phys. Rev. Lett.*, 1999, **83**, 3772–3775.

33 F. Liu, Y. Lu, L. Pieuchot, T. Dhavale and G. Jedd, *Dev. Cell*, 2011, **21**, 457–468.

34 F. J. Vizeacoumar, J. C. Torres-Guzman, D. Bouard, J. D. Aitchison and R. A. Rachubinski, *Mol. Biol. Cell*, 2004, **15**, 665–677.

35 L. Golubovic and M. Golubovic, *Phys. Rev. E: Stat. Phys., Plasmas, Fluids, Relat. Interdiscip. Top.*, 1997, **56**, 3219–3230.

36 D. E. Moody and J. K. Reddy, *J. Cell Biol.*, 1976, **71**, 768–780.

37 J. Iwata, J. Ezaki, M. Komatsu, S. Yokota, T. Ueno, I. Tanida, T. Chiba, K. Tanaka and E. Kominami, *J. Biol. Chem.*, 2006, **281**, 4035–4041.

38 H. W. Platta and R. Erdmann, *Trends Cell Biol.*, 2007, **17**, 474–484.

39 M. Veenhuis, A. Douma, W. Harder and M. Osumi, *Arch. Microbiol.*, 1983, **134**, 193–203.

40 N. A. Bonekamp, S. Grille, M. J. Cardoso, M. Almeida, M. Aroso, S. Gomes, A. C. Magalhaes, D. Ribeiro, M. Islinger and M. Schrader, *PLoS One*, 2013, **8**, e53424.

41 J. J. Sieber, K. I. Willig, R. Heintzmann, S. W. Hell and T. Lang, *Biophys. J.*, 2006, **90**, 2843–2951.

42 T. Lamark, M. Perander, H. Outzen, K. Kristiansen, A. Overvatn, E. Michaelsen, G. Bjorkoy and T. Johansen, *J. Biol. Chem.*, 2003, **278**, 34568–34581.